JOURNAL OF NANO- AND ELECTRONIC PHYSICS
Vol. **16** No 1, 01002(6pp) (2024)

ЖУРНАЛ НАНО- ТА ЕЛЕКТРОННОЇ ФІЗИКИ
Том **16** № 1, 01002(6cc) (2024)

OPEN ACCESS

REGULAR ARTICLE

A Spiral Wire_coil Wideband Metasurface Absorber with Ultrathin and Flexible Feature for Microwave Applications

G.H. Mebarki*✉, N. Benmostefa

Abou Baker Belgaid University, Algeria

(Received 09 November 2023; revised manuscript received 10 February 2024; published online 28 February 2024)

This current work presents the design and the experimental validation of an ultrathin a spiral Wire_coil wideband conformal metamaterial absorber. The proposed absorber is comprised of Wire_coil resonators on the upper side of the flexible substrate and a copper metal film on the lower side, which are separated by flexible PET (terephthalate). More than 90 percent of the frequency range from 16.5 GHz to 27.3 GHz was determined to be absorbed through testing. Due to its symmetrical form, the suggested absorber is indifferent to polarization. The absorber's unit cell is meant to be as small as possible with dimensions of $0.19\ \lambda_0 \times 0.19\ \lambda_0$ (where λ_0 is the wavelength at 16.5 GHz) .Using a parametric analysis and an equivalent circuit model, the absorber's wideband absorption mechanism was investigated further. Moreover, by varying the incidence angle up to 50 degrees, the bandwidth exhibits an effective absorption response for both TE and TM polarizations. Both simulation and experiment yield very similar results. Because of its simple design, the proposed absorber has potential properties for use in scientific and radio diffusion systems, offering outstanding performance.

Keywords: Metamaterial, Absorber, Flexible, Ultrathin, Spiral Wire_coil.

DOI: 10.21272/jnep.16(1).01002 PACS number: 42.25.Bs

1. INTRODUCTION

Metamaterial (MMs) is a precision-engineered periodic structure consisting using subwavelength components with exceptional electromagnetic features. It is employed in a wide range of applications from microwave to terahertz frequency [1]. Furthermore, it's attain their characteristics from their recently constructed structures, not from the properties of their original materials. Their exact structure, geometry, size, orientation, and arrangement offer them intelligent features capable of manipulating EM waves: blocking, absorbing, amplifying, or bending waves to obtain advantages that beyond what traditional materials can do [2]. As indicated by Kirchhoff's law of thermal radiation, the absorptivity of an object is equal to its thermal emissivity. For accurate non-contact temperature measurement and heat transfer calculations, a comprehensive knowledge of the emissivity of numerous materials is required. Before calculating a thermal emitter's emissivity, it is standard practice to investigate its absorption characteristics [3]. Metamaterial-based absorbers (MMA) promise a future of lightweight, ultra-thin, and flexible materials that may literally be set to any surface to provide the essential absorption qualities at radar, infrared, and even optical frequencies [4].The MMA is made by processing and designing the form, size, and manner of merging artificial composite materials in order to achieve effective absorption in a very narrow or large frequency spectrum. Metamaterials are now employed in industrial and military applications, such as communication, stealth, and thermal detection systems. Thus, MMA research is critical for improving the performance of these applications [5]. Since the 2008 [6] proposal of a metal-dielectric electromagnetic material named "perfect metamaterial absorber" in the gigahertz (GHz) regime, many scientists and engineers have been particularly interested in the creation of thin electromagnetic metamaterial absorber (MMA). The pressing need for significantly smaller and lighter MM absorbers will necessitate their invention [7, 8]. A lot of novel efforts on the MMA have so far focused on increasing the bandwidth, reducing the thickness, achieving polarization-insensitive absorption, and making it simple to coat the scatterer [9]. By investigating the use of flexible dielectric materials, previous issues were effectively addressed, and this strategy was eventually applied to MMA. Due to a Teflon coating, Yoo and al. [10]designed a low-frequency MM absorber that is both elastic and flexible. Depending on the number of snake-bar constructions employed, it specially designed for two absorption peaks around 2 GHz and 400 MHz. Tak and al. [11] presented a wearable metamaterial microwave absorber (WMMA) with two absorptivity maxima at 9 and 9.8 GHz for indoor radar clear applications. Additionally, it is polarization and deformation resistant. Y.K. Awasthi and al. [12] developed ultra-thin single-layer metasurface absorber has been without the need for resistive layers or components, a 40% fractional bandwidth with a bandwidth of 10 to 15 GHz and an overall absorption of more than 90%. S. Kalraiya and all [13] investigated flexible MM absorbers which consist of a slotted sector and a circle that are loaded with four lumped resistors in between. The MMA may achieve a frequency band that spans 3.90 GHz to 10.5 GHz with a fractional band of 92 percent.

* Correspondence e-mail: mebarkighada96@gmail.com

Cite this article as: G.H. Mebarki et al., *J. Nano- Electron. Phys.* 16 No 1, 01002 (2024) https://doi.org/10.21272/jnep.16(1).01002

S. Lai and all [7] reports a metamaterial absorber Based on the APS-PSO algorithm this design use flexible and optically transparent wave-absorbing material ITO-PET (polyethylene terephthalate) and it's obtain an absorptance of over 90% in the 5.06–9.01 GHz range.

Recently; different techniques have been proposed in the design of gigahertz and terahertz metamaterial absorbers to enlarge the absorption bandwidth, including the use of multi-resonance mechanisms, fractal structures, multilayer, magnetic media, and loading lumped elements [14]. In this study, an ultra-thin single-layer wideband metasurface absorber with absorption more than 90% across a bandwidth of 16.5 to 27.3 GHz is suggested.

The geometry of the absorber's unit cell includes. A spiral Wire coil is made with 35 μm copper cladding on top of a 1.6-mm thick PET dielectric substrate. The simulated results correspond well with the observed data. The different characteristics of the suggested wideband conformal absorber are compared to the previously published wideband absorber structure, as given in Table 2, and it is clearly shown that the unit cell of the suggested absorber is compact and achieves a broader bandwidth with single layer, with simple structure and without any lumped resistors. This paper is divided into many parts. Section II describes the proposed structure's design technique. Section III includes simulated Result, as well as parametric variation. Section IV shows the experimental results. Sec. V discusses the conclusion.

2. DESIGN METHODOLOGY AND THEORICAL SIMULATION

The Fig. 1 depicts the 3d side and top view of the proposed unit cell of the designed flexible wideband MMA with single layer which consist of 3 turn of split wire resonator on the top side fixed on terephthalate (PET) substrate ($\varepsilon_r = 3.5$ and $tan\delta = 0.015$) with thickness of 1.6 mm. The PET used as dielectric substrate because it provides greater flexibility with low cost.

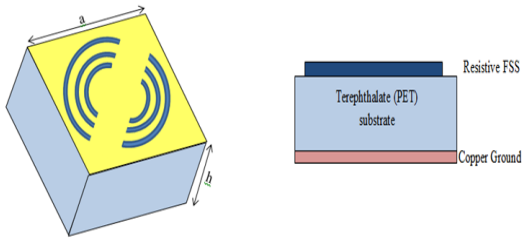

(a) (b)

Fig. 1 – The proposed MM absorber's unit cell, presented from a Two views. (a) A view from the side. (b) A look at the front

The Table 1 listed the detailed structural information of the proposed MMA. The absorptivity (A) is defined in Eq. (1) as:

$$A(\omega) = 1 - |S_{11}(\omega)|^2 - |S_{21}(\omega)|^2, \quad (1)$$

where $S_{11}(\omega)$ and $S_{21}(\omega)$ are the reflection and transmission coefficients respectively. Due to the totally reflection of the copper ground plane, the transmission coefficient $S_{21}(\omega)$ is zero. Therefore, the absorptivity can be rewritten as: $A(\omega) = 1 - |S_{11}(\omega)|^2$. The suggested design's unit cell architecture has been logically simulated using the commercial software CST MICROWAVE STUDIO™2021. The open-space boundary condition is applied in the z direction (the propagation of the EM wave along the z-axis), and the unit cell boundary conditions are used in the x and y directions.

Table 1 – Dimensions and parameters of the MA

Name	Value	Description
a	3.5 mm	MMA size
E	180°	Wire_coil_end_angle
S	90°	Wire_coil_start_angle
Angle	45°	Wire_coil_angle
N	3	Wire_coil_turns
h	1.6 mm	Thickness of substrate
g	0.4	Wire_coil_progress
R0	0.3 mm	Inner Radius of Spiral
Ws	0.1 mm	Trace Width
t	0.035 mm	Wire_coil_trace_height

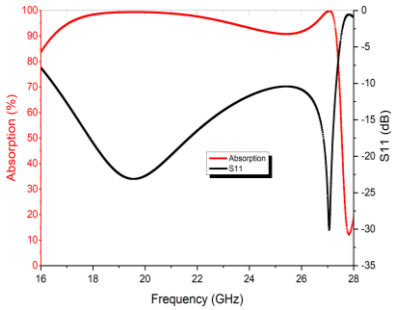

Fig. 2 – SimulatedS11 and absorption of the flexible absorber

In general, we measure the bandwidth of broadband absorbers with an efficiency of absorption more than 90%. The absorption and reflection curves for the proposed MA at positive incidence are shown in Fig. 2. The frequency bandwidth for up to 90% absorption is from 16.5 to 27.3 GHz. The absolute bandwidth is 10.8 GHz and the fractional bandwidth is described as, $W_{FRA} = 2\,(f_U - f_L)/(f_U + f_L)$, where f_U and f_L are the upper and lower frequency range limitations for absorption over 90%. respectively, resulting in a W_{FRA} around 50%, which performs the ultra-wideband absorption criteria. The absorber's thickness is just 1.67 mm, which is 0.09 times the working wavelength of the lowest absorption frequency (16.5 GHz) and answers the subwavelength structural requirements. As a result, the proposed work is a broadband ultra-thin metamaterial absorber.

2.1 Numerical Solution

2.1.1. Normalized Impedence and Metamaterial Propriety

Fig. 3a depicts the normalized input impedance (Zin) of the planned absorber, which was calculated using scattering parameters from Eq. (2). At the absorption frequency band, the real values of the normalized input impedance are nearly unity (around 1), while the imaginary values are close to zero, i.e., the absorber's input imped-

ance is nearly equal to the impedance of free space ($377 + j0$), so that less power is reflected from the structure; thus, maximum absorptivity occurs at the desired frequency band.

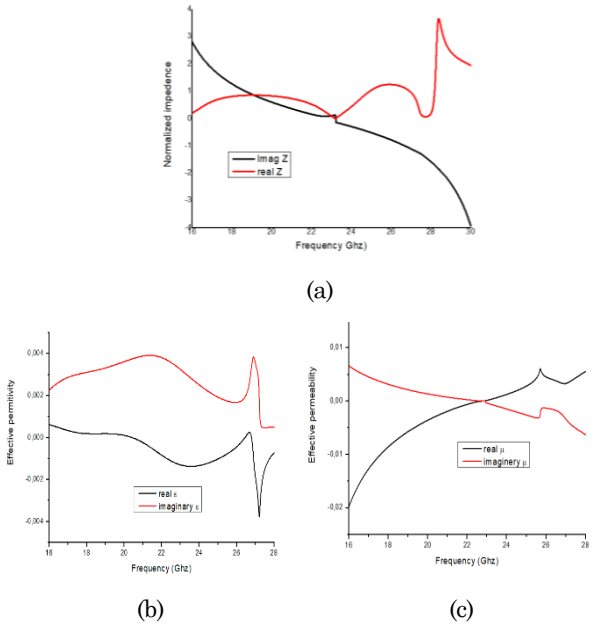

Fig. 3 – (a) The normalized impedance of the proposed absorber at normal incidence. (b), (c) Effective permitivity and permittivity of the designed absorber

Fig. 3(b) and (c) show the effective permeability (μ_{eff}) and permittivity (ε_{eff}) of the proposed structure in order to better understand the absorption character. These were generated using the following equations [15].

$$Z(f) = \sqrt{\frac{(1+S_{11}(f))^2 - S_{21}{}^2(f)}{(1-S_{11}(f))^2 - S_{21}{}^2(f)}} \quad (2)$$

$$\varepsilon_{eff}(f) = \frac{c}{j\pi f d}\left(\frac{1-S_{21}-S_{11}}{1+S_{21}+S_{11}}\right) \quad (3)$$

$$\mu_{eff}(f) = \frac{c}{j\pi f d}\left(\frac{1-S_{21}+S_{11}}{1+S_{21}-S_{11}}\right). \quad (4)$$

At absorption frequencies, the real part of both values approaches zero ($\varepsilon_{eff} < -0.004$; $\mu_{eff} < 0.02$), indicating no reflection. In other way the real components of permittivity and permeability have almost opposite signs in the absorption band, there is no transmission.

2.1.2. Electric Field, Magnetic Field, and Surface Current Distributions

In order to fully comprehend the physical process of the device's wideband absorption, the electric field and the magnetic field distribution at the two absorption points was measured. According to the demonstrating results in Fig. 2, the highest absorptivity values are at 19.32 and 27.1 GHz. Fig. 4 and 5 shows the electric filed and surface current distributions of the top layer of MMA at two absorption frequencies (19.32 and 27.1 GHz) to provide a better understanding of the absorption process.

In Fig. 4(a), the distribution of E- field and H-field at 19.32 GHz is mostly centered on the outer boundaries of the structure. At 27.1 GHz (Fig. 4(b)), the E-field and the H-field intensity is mostly concentrated around the unit cell, it indicates that the coupling between the inner and outer copper cross patterns. This simulation result proves the importance of the SRR shape to obtaining the large absorption bandwidth.

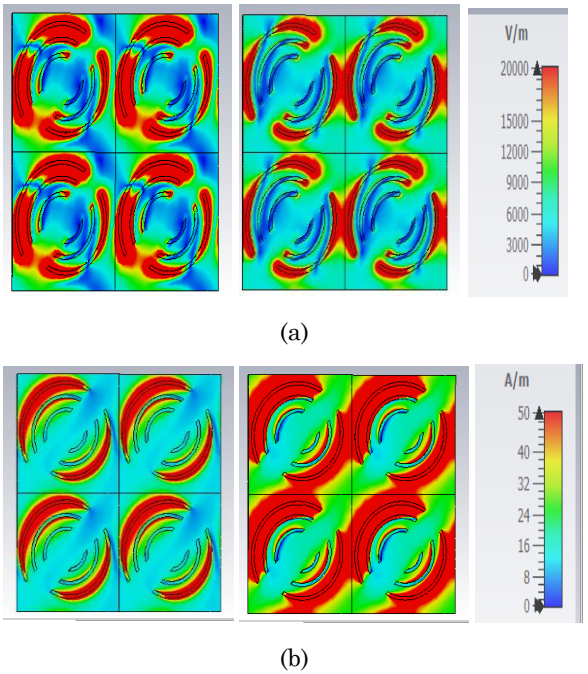

Fig. 4 – Electric field; and magnetic field distribution at (a) at 19.31 and (b) at 27.1 GHz respectively

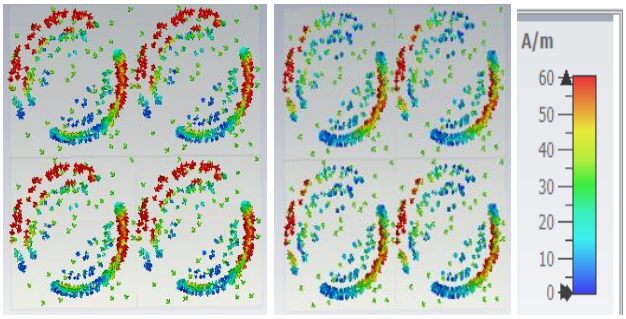

Fig. 5 – Surface current destribution distribution at (a) 19.31 and (b) 27.1 GHz

Surface current distribution at 19.31 GHz and 27.1 GHz has been exhibited to explain the absorption phenomena of the suggested absorber, as shown in Fig. 5. According to this Figure, the majority of the current distribution was discovered all over the surface of adjoining SRR witch is responsible for the appearance of the absorption band. Furthermore, the surface currents in the top resistive layer and metal ground plane are antiparallel to each other, resulting in magnetic resonance. It is also noted that the intensity of the current in the bottom layer is much lower than in the top resistive layer, implying that the majority of the energy is wasted in the top resistive layer before reaching the bottom layer. As a result, instead of dielectric loss, the resistive top layer is responsible for wideband absorption.

2.1.3. Polarization and Incident Angle Stability

As shown in Fig. 6, the absorptivity of the prototype is tested at several polarization angles to verify the proposed wideband absorber's polarization-insensitive performance. In this case, the electric field and magnetic field are at right angles to the x and y axes, while the microwave propagates into the z axis. It's worth noting that the absorption curves coincide identically for all polarization orientations. This is because the unit cell of the flexible absorber's surface resonance pattern is rotationally symmetric around its central axis. Thus, the suggested structure exhibits remarkable polarization-independent absorption performance.

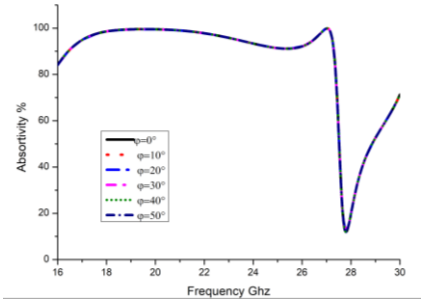

Fig. 6 – Dependence of the absorption performance on the polarization angle in case of normal incidence

The preceding study shows that the proposed absorber is effective throughout a broad range of polarization and incidence angle, in both the TE and TM directions.

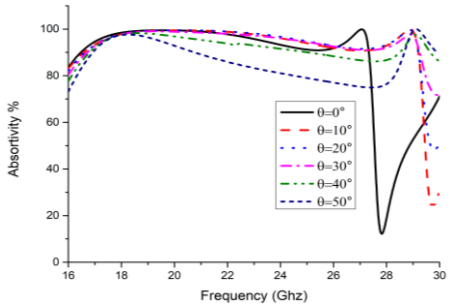

(a)

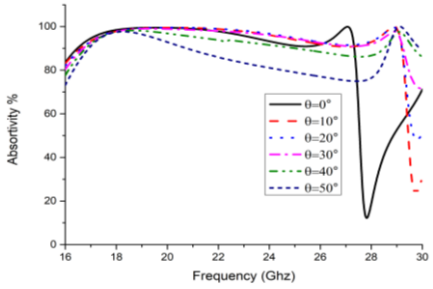

(b)

Fig. 7 – Absorption spectra of the MM absorber with various incident angle for TE (a) and TM (b) polarizations

Fig. 7 depicts the TM and TE polarizations absorption responses for a range (from 0° to 50°) of oblique incidence angles φ set to 0°. Fig. 7.a displays the oblique angle shifts under TE polarization. We use rotational displacement to change the magnetic field and wave propagation vector while keeping the electric field direction constant.

Fig. 7.b depicts the TM polarization produced by varying the electric field and wave propagation vector by an angle while keeping the magnetic field direction constant. This Figure demonstrates that the proposed single -layer flexible MMA design is an effective wide-angle absorber, with observed absorption levels of 70% up to 50° under TE polarization and exactly the same way under TM polarization.

2.1.4. The Substrate Thikness

The next Figure presents the absorptivity as a function of substrate thickness (h) from 0.8 mm to 1.6 mm, and it is shown that the absorption bandwidth decreased significantly as h increased. However, its conformality degrades with increasing substrate thickness. To maximize the available absorption bandwidth, a thin, flexible substrate (1.6 mm) was used.

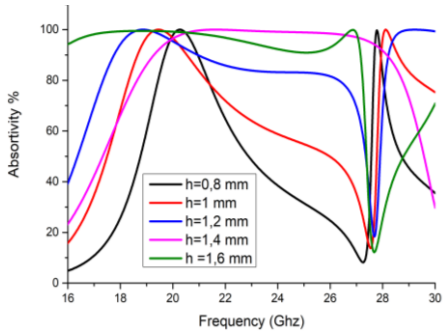

Fig. 8 – Absorption results of the PMA with different subtract thicknesses of h

2.1.5. Equivalent Transmission Line Model of Absorber

Fig. 9 is an equivalent circuit model that combines transmission line theory (Free space and the dielectric layers are considered as transmission lines) and can be used to describe the proposed structure [16]. The proposed absorber was simulated using Keysight's Path-Wave Advanced Design System (ADS) software. The outside ring, the extra component attached to it, and the inner split ring altogether comprise an RLC circuit linked in parallel by the coupling capacitance [17]. Eq. (5) was used to compute the inductances L_1, L_2, and L_3 from the outer ring, outer ring extra components, and inner rings, respectively. [18].

$$L_{ms} = 0.005080L[\ln\left(\frac{2l}{W+D}\right) + 0.5 + 0.2235\left(\frac{W+D}{l}\right)]. \quad (5)$$

The variable L_{ms} represents the inductance per unit length of the microstrip, measured in microhenries (μH). The variable l denotes the length of the strip, measured in inches. W represents the width of the strip, also measured in inches. Lastly, D represents the distance between the strip-line and the ground plane.

Eq. (6) calculates the associated capacitances C_1, C_2, and C_3 for lower, middle, and upper frequencies, where f is the resonance frequency [15].

$$c = \frac{1}{4\pi^2 f^2 L_{ms}}, \quad (6)$$

Where f is the frequency at which resonance is requested. In order to calculate the input impedance needed by the unit cell construction, the ohmic loss (R_o) of the region contained by SRRs and the dielectric loss (R_d) of the substrate must be taken into account.

$$R_0 = \frac{Cell\ area}{metalic\ area\ of\ SRR}\left(\frac{1}{\sigma\delta}\right). \quad (7)$$

For a metallic SRR, we get where $\sigma$the conductivity is, δ is the skin depth, and $\frac{1}{\sigma\delta}$ is the surface resistance of the non-metal region circumscribed by the resonator. The total resistance should be connected with the surface resistance (for each resonance frequency) since the surface resistance affects the absorption characteristics of the unit cell as:

$$R = R_0\left(\frac{P}{S}\right)^2, \quad (8)$$

S is the entire length of the resonator, and P is the period of the unit cell. The dielectric loss (R_d) may be simply calculated from simulation data because of the SRR's unloaded capacitance. R_d was considered a variable resistor that could be modified in the simulator to produce the required S values, which greatly simplified the calculation [19].

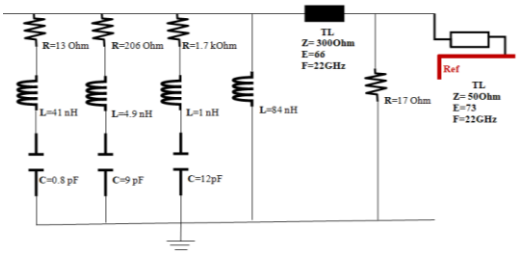

Fig. 9 – Equivalent circuit topology for geometry of the PMA

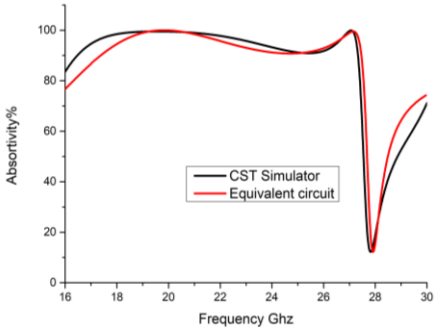

Fig. 10 – Comparison between the CST and ADS numerical simulations of absorption.

The determination of the equivalent resistance in an RLC circuit requires the adjustment of the absortivity to observe changes in its magnitude, both in terms of increase and decrease. The estimated parameters were further adjusted in order to approximate a comparable S_{11} curve as obtained from CST. Fig. 10 illustrates the absortivity parameter obtained from both the CST and ADS simulations.

2.1.6. Comparison Table

At last, a comparison is made between the proposed metamaterial absorber based wire coil and the other flexible MMA absorber based on different shape of resonators. Table2 summarizes the comparison and demonstrates how the suggested work is novel due to its frequency selection, low profile structure, larger bandwidth, simple design and polarization stability, in addition to its flexibility.

Table 2 – Comparison analysis with state of the art

MA	Total Thikness (mm)	Bandwidth Absortivity spans (GHz)	Flexible	Design propriety
[20]	3.8	4.8 to 11.1 (6.3)	NO	Circuit equivalent based on IOT
[21]	8	8.2 to 16 (7.8)	NO	Polymide film, PET and Ground separated by PMI layers
[13]	7.5	3.9 to 10.5 (6.6)	YES	circle and a slotted sector, loaded with lumped resistors
[22]	2.7	6.68 to 18 (11.32)	Yes	Copper, rubber substrate, PET , resistive film
[23]	3.302	7.6 to 18.3 (10.35)	YES	silicone rubber,polymide, resistive FSS with fours lumped elements
[24]	8.23	3.25 to 16.3 (10.35)	YES	Foam, PET, cross-shaped resonator loaded with lumped resistors
Proposed design	1.67	16.5 to 27.3 (10.8)	YES	PET, spiral coil SRR

3. CONCLUSION

A metamaterial absorber was constructed in this study employing a spiral wire coil patterning on a single layer of PET flexible substrate. The absorber performs well, as shown by evaluates which correspond with the mathematical results; over 90% absorption in the 16.3 to 27.5 GHz spectrum. Furthermore, the proposed MA is polarization insensitive and has a wide incidence angle range for both TE and TM modes. The impact of modifying the geometric properties of the MA on its operating frequency and absorption was studied and explained. The excellent performance may be maintained, however, if the geometric parameter changes within a certain range.

REFERENCES

1. H. Wang, et al., *TrAC - Trends Anal. Chem.* **158**, 116888 (2023).
2. M. Momeni-Nasab, S.M. Bidoki, M. Hadizadeh, M. Movahhedi, *AEU - Int. J. Electron. Commun.* **123**, 153259 (2020).
3. Y.I. Abdulkarim, et al., *Res. Phys.* **26**, 104344 (2021).
4. G. Singh, H. Sheokand, K. Chaudhary, K. Vaibhav Srivastava, J. Ramkumar, S.A. Ramakrishna, *J. Phys. D. Appl. Phys.* **52** No 38, (2019).
5. P. Yu, et al., *Adv. Opt. Mater.* **7** No 3, 1800995 (2019).
6. N.I. Landy, S. Sajuyigbe, J.J.Mock, D.R. Smith, W.J. Padilla, *Phys. Rev. Lett.* **100** No 20, 207402 (2008).
7. S. Lai, G. Liu, Y. Guo, Y. Liu, *Symmetry (Basel).* **14** No 10, 2217 (2022).
8. P. Stability, H. Zhai, C. Zhan, Z. Li, C. Liang, S. Member, *IEEE Anten. Wirel. Propag. Lett.* **14**, 241 (2015).
9. M. Wang, B. Weng, J. Zhao, X. Zhao, *Appl. Phys. A Mater. Sci. Process.* **123** No 6, 434 (2017).
10. Y.J. Yoo, et al., *Appl. Phys. Lett.* **105** N 4, 041902 (2014).
11. J. Tak, J. Choi, *IEEE Antennas Wirel. Propag. Lett.* **16** No C, 784 (2017).
12. G. Deng, et al., *Nanoscale Res. Lett.* **15** No 1, 217 (2020).
13. S. Kalraiya, R.K. Chaudhary, M.A. Abdalla, *J. Appl. Phys.* **125** No 13, 134904 (2019).
14. S.J. Li, et al., *Nanoscale Res. Lett.* **13**, 386 (2018).
15. M.L. Hakim, et al., *Nanomaterials* **13** No 2, 222 (2023).
16. F. Costa, S. Genovesi, A. Monorchio, G. Manara, *IEEE Trans. Anten. Propag.* **61** No 3, 1201 (2013).
17. Microwave_Solid_State_Circuit_Design_By_Bahl.Pdf.
18. S. Hannan, M.T. Islam, M.R.I. Faruque, M.E.H. Chowdhury, F. Musharavati, *Sci. Rep.* **11** No 1, 13791 (2021).
19. F. Costa, A. Kazemzadeh, S. Genovesi, A. Monorchio, *Resistor* **37** No 1, 1 (2016).
20. R. Deng, et al., *Materials (Basel)* **11** No 1, 107 (2018).
21. H.Y. Huang, *Nanotechnology* 1 (2017).
22. L.L. Wang, S. Bin Liu, H.F. Zhang, X.K. Kong, L.L. Liu, *J. Electromagn. Waves Appl.* **31** No 13, 1216 (2017).
23. H. Chen, et al., *Mater. Res. Exp.* **5** No 1, 015804 (2018).
24. S. Kalraiya, R.K. Chaudhary, M.A. Abdalla, *AEU - Int. J. Electron. Commun.* **143**, 154033 (2022).

Широкосмуговий метаповерхневий поглинач із ультратонкими та гнучкими функціями для мікрохвильових застосувань

G.H. Mebarki, N. Benmostefa

Abou Baker Belgaid University, Algeria

У даній роботі представлено дизайн та експериментальне підтвердження ультратонкого спірального широкосмугового конформного метаматеріального поглинача Wire_coil. Запропонований поглинач складається з резонаторів Wire_coil на верхній стороні гнучкої підкладки та мідної металевої плівки на нижній стороні, які розділені гнучким ПЕТ (терефталатом). Більше 90% діапазону частот від 16,5 ГГц до 27,3 ГГц виявилося поглиненим під час тестування. Завдяки своїй симетричній формі запропонований поглинач нечутливий до поляризації. Елементарна комірка поглинача повинна бути якомога меншою з розмірами $0.19\,\lambda_0 \times 0.19\,\lambda_0$ (де λ_0 — довжина хвилі на 16,5 ГГц). Використовуючи параметричний аналіз і модель еквівалентної схеми, механізм широкосмугового поглинання поглинача був визначений досліджено далі. Крім того, змінюючи кут падіння до 50 градусів, смуга пропускання демонструє ефективну реакцію поглинання як для TE, так і для TM поляризацій. Моделювання і експеримент дають дуже схожі результати. Завдяки своїй простій конструкції запропонований поглинач має потенційні властивості для використання в наукових і радіодифузійних системах, забезпечуючи високу продуктивність.

Ключові слова: Метаматеріал, Абсорбер, Гнучка ультратонка спіральна дротяна котушка.